NANO LETTERS

Letter

pubs.acs.org/NanoLett

Cooperative Plasmonic Effect of Ag and Au Nanoparticles on Enhancing Performance of Polymer Solar Cells

Luyao Lu, Zhiqiang Luo, Tao Xu, and Luping Yu*

Department of Chemistry and The James Franck Institute, The University of Chicago, 929 E. 57th Street, Chicago, Illinois 60637, United States

Supporting Information

ABSTRACT: This article describes a cooperative plasmonic effect on improving the performance of polymer bulk heterojunction solar cells. When mixed Ag and Au nanoparticles are incorporated into the anode buffer layer, dual nanoparticles show superior behavior on enhancing light absorption in comparison with single nanoparticles, which led to the realization of a polymer solar cell with a power conversion efficiency of 8.67%, accounting for a 20% enhancement. The cooperative plasmonic effect aroused from dual resonance enhancement of two different nanoparticles. The idea was further unraveled by comparing Au nanorods with Au nanoparticles for solar cell application. Detailed studies shed light into the influence of plasmonic nanostructures on exciton generation, dissociation, and charge recombination and transport inside thin film devices.

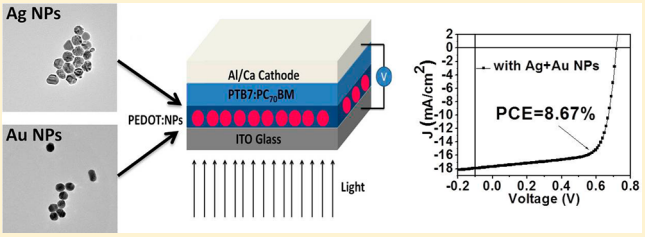

KEYWORDS: *Polymer solar cells, silver and gold nanoparticles, plasmonic effect, impedance spectroscopy, gold nanorods*

Organic bulk heterojunction (BHJ) solar cells with a bicontinuous interpenetrating network between the polymer donor and fullerene acceptor exhibit potential advantages as lightweight, flexible, large area devices and in the low cost roll to roll fabrication methods.[1−4] These devices are envisioned as a very promising candidate to harvest solar energy. Multidisciplinary efforts have been taken in recent years to pursue polymer solar cells exhibiting high power conversion efficiency (PCE), such as rational designs of low-bandgap conjugated polymers,[5−10] optimization of film morphology,[11−19] and developing new device architectures.[20−23] These efforts have led to BHJ solar cells with PCEs close to 9% in small area devices.[24−27]

Although the perceived advantages of these solar cells are attractive, the performance of polymer BHJ solar cells is still limited by insufficient light absorption and low charge carrier mobility within the thin films.[2,28] Different approaches were taken to enhance the light absorption with the cautions to optimize cell absorption without increasing the thickness of the active layer, so to avoid the increase in charge recombination.[28,29] Recently, metallic nanoparticles (NPs) were introduced into organic photovoltaic (OPV) devices for highly improved light harvesting by utilizing the localized surface plasmonic resonances (LSPR) of metallic NPs.[29−36] However, only a handful reports showed a solar cell PCE higher than 8% by incorporating metallic NPs into OPV devices,[37] and the influence of NPs on charge separation and transport inside high efficiency BHJ solar cells still needs to be explored in depth.

Here we report a cooperative PCE enhancement of 20% by simply adding Ag and Au mixture (dual NPs) into photovoltaic devices fabricated from our champion donor polymer polythieno[3,4-b]-thiophene/benzodithiophene (PTB7) and [6,6]-phenyl C_{71}-butyric acid methyl ester ($PC_{70}BM$). We show here that incorporation of dual NPs exhibits the following advantages: (1) broader light absorption enhancement than single NPs; (2) enhanced exciton generation rate and dissociation efficiency; and (3) increased charge carrier density and lifetime. As a result, we achieved a high PCE of 8.67% for our BHJ polymer solar cells.

Figure 1 shows molecular structures of PTB7 and $PC_{70}BM$, OPV device structure, and transmission electron microscopy (TEM) images of Ag and Au NPs used in this paper. The TEM images indicate that the sizes of both Ag and Au NPs are around 40 to 50 nm, which are comparable to the thickness of the PEDOT layer (60 nm). Therefore it is safe to assume that NPs are imbedded within PEDOT layer and LSPR are induced near the active layer of our devices. This assumption is also confirmed by atomic force microscopy (AFM) images. Figure 2 illustrates AFM images of PEDOT:PSS with and without dual NPs. The root-mean-squared (RMS) roughness of PEDOT:PSS layer on ITO glass is measured to be 1.02 nm while PEDOT:PSS mixed with dual NPs exhibits exactly the same RMS roughness. Thus we could anticipate that all the NPs are located within the PEDOT layer so that the RMS roughness remains unchanged.

To clarify the effect of dual NPs in OPV devices, we first optimized solar cell performance with each type of NPs, and then we investigated the effect of dual NPs. Solar cells with the

Received: September 14, 2012
Revised: November 22, 2012
Published: December 13, 2012

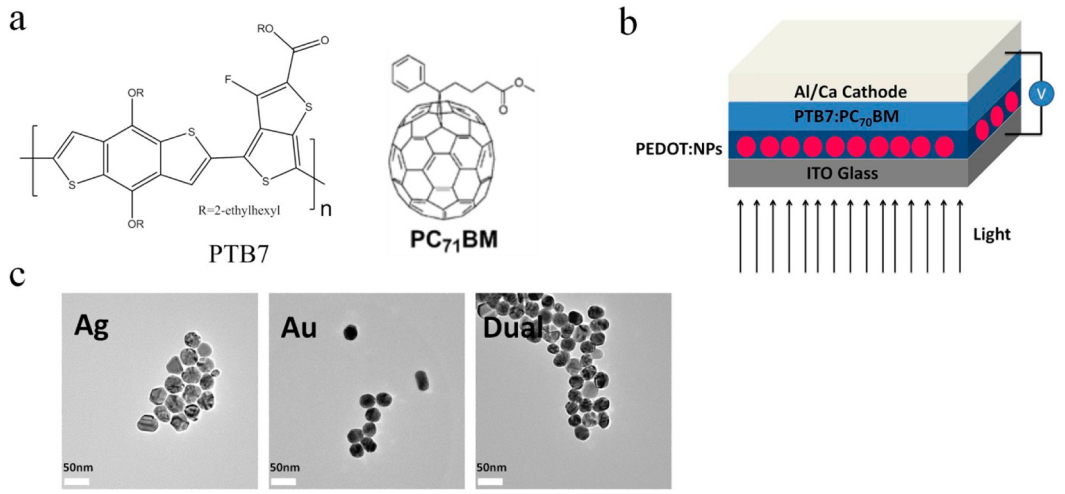

Figure 1. (a) Molecular structures of PTB7 and $PC_{70}BM$. (b) Device structure of the solar cell used in this work. (c) TEM images of Ag, Au, and dual NPs.

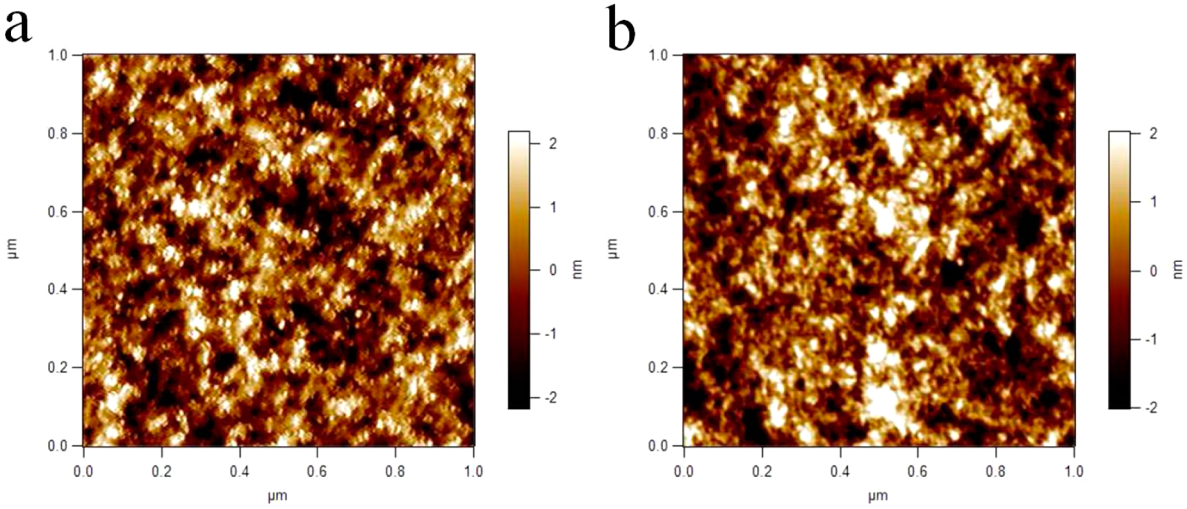

Figure 2. (a) AFM images of PEDOT with dual NPs. (b) AFM images of PEDOT without dual NPs.

structure of ITO/PEDOT:PSS with NPs/PTB7:$PC_{70}BM$/Ca/Al were fabricated and measured under AM 1.5G illumination at 100 mW/cm^2. Corresponding current density versus voltage (J–V) curve of PTB7:$PC_{70}BM$ without NPs, with Ag NPs, with Au NPs, and with dual NPs is shown in Figure 3a. Table 1 provides a summary of photovoltaic parameters. After incorporating Ag NPs into PEDOT:PSS layer, open-circuit voltage (V_{oc}) remained nearly the same, short-circuit current density (J_{sc}) increased from 15.0 to 16.4 mA/cm^2, FF increased from 67.1 to 68.8%. As a result, PCE enhanced from 7.25 to 8.01%. Incorporating Au NPs into PEDOT layer shows similar improvement. V_{oc} remained unchanged, J_{sc} improved to 16.7 mA/cm^2 and FF enhanced to 68.8%, leading to a PCE of 8.16%. Both Ag and Au NPs exhibit around 10% enhancement of PCE due to the notable enhanced J_{sc} and improved FF.

After that, we studied the effect of dual NPs by simply mixing Ag and Au NPs of optimized conditions together into PEDOT:PSS layer. Very interestingly, devices with dual NPs showed much better solar cell performance, J_{sc} further improved to 17.7 mA/cm^2 and FF enhanced to 69.0%, resulting in a promising PCE of 8.67%. Average solar cell parameters over 10 identical devices are summarized in Supporting Information Table S1. Typically, devices with dual NPs showed mean V_{oc} at 0.71 ± 0.01 V, J_{sc} at 17.6 ± 0.18 mA/cm^2, FF at 68.7 ± 0.37%. The average PCEs for solar cells with Ag NPs, Au NPs, and dual NPs are 7.96 ± 0.09, 8.06 ± 0.09, 8.56 ± 0.14%, respectively. The small standard deviations indicate good reliability and reproducibility of our results. Besides, the series resistance (R_s) of devices with NPs decreased compared with the control device (summarized in Supporting Information Table S2). Especially, the R_s of solar cells with dual NPs reduced from 6.76 (without NPs) to 4.44 Ω cm^2 (with dual NPs). Consequently, FF increased from 67.1 (without NPs) to 69.0% (with dual NPs) in this work.

External quantum efficiency (EQE) measurements of four different solar cells are first conducted to better elucidate improved J_{sc}. Figure 3b depicts the corresponding EQE spectra. For device with dual NPs, EQE increased over a broad wavelength range from 350 to 750 nm while for device with Ag NPs, EQE mainly increased from 350 to 600 nm and for device with Au NPs, EQE increased from 500 to 750 nm. The maximum EQE values for Ag NPs, Au NPs and dual NPs devices are 81, 80, and 82%, respectively. The integrated J_{sc} values from our EQE spectrum for four devices are 14.8, 16.2, 16.4, and 17.4 mA/cm^2, respectively. The difference between

dx.doi.org/10.1021/nl3034398 | Nano Lett. 2013, 13, 59–64

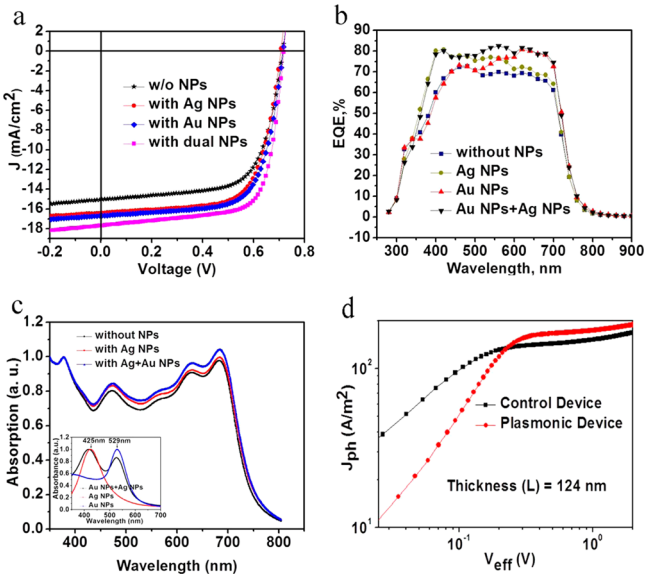

Figure 3. (a) Current–voltage characteristics of solar cells with and without NPs. (b) EQE spectra of PTB7/$PC_{70}BM$ with and without NPs. (c) UV–vis absorption spectra of PTB7/$PC_{70}BM$ without NPs, with Ag NPs and with dual NPs. Inset: UV–vis absorption spectrum of NPs in water. (d) Potocurrent density (J_{ph})versus effective voltage (V_{eff}) characteristics of the control and dual NPs devices.

Table 1. Photovoltaic Parameters of Solar Cells with Different NPs under AM 1.5G Illumination at 100 mW/cm^2

NPs	J_{sc} (mA/cm^2)	V_{oc} (V)	FF (%)	PCE (%)
no	15.0	0.72	67.1	7.25
Ag	16.4	0.71	68.8	8.01
Au	16.7	0.71	68.8	8.16
dual	17.7	0.71	69.0	8.67

intergrated J_{sc} and measured J_{sc} are within 3%, indicating good accuracy of our OPV measurement.

To better illustrate the J_{sc} enhancement, we also performed UV–vis absorption measurements of solar cells with and without NPs. The absorption spectrum is shown in Figure 3c. We can tell that the absorption of PTB7:$PC_{70}BM$ cell in the region of 420 to 600 nm is enhanced after incorporation of Ag NPs, further incorporation of Au NPs improved the absorption from 520 to 750 nm. It is clear from EQE spectra and UV–vis absorption spectra that dual NPs shows broader absorption enhancement region than single NPs. The enhanced absorption is in good agreement with the plasmonic resonance region of Ag and Au NPs (inset of Figure 3c). On the basis of EQE and UV–vis absorption results, it is clear that dual NPs greatly broaden the wavelength range for absorption enhancement compared with either Ag or Au NPs.

To explore the effects of NPs on exciton generation and dissociation, we determined the maximum exciton generation rate (G_{max}) and exciton dissociation probabilities $P(E,T)$ of our OPV devices. Figure 3d reveals the effect of LSPR on photocurrent density (J_{ph}) versus effective voltage (V_{eff}). J_{ph} is determined as $J_{ph} = J_L - J_D$, where J_L and J_D are the current density under illumination and in the dark, respectively. V_{eff} is determined as $V_{eff} = V_0 - V_a$, where V_0 is the voltage at which $J_{ph} = 0$ and V_a is the applied bias voltage.[38] Figure 3d clearly shows that J_{ph} increases linearly at low V_{eff} range and saturates at a high V_{eff} (i.e., $V_{eff} = 2$ V). Assuming that all the photogenerated excitons are dissociated into free charge carriers and collected by electrodes afterward at a high V_{eff} region,[39,40] saturation current density (J_{sat}) is then only limited by total amount of absorbed incident photons. G_{max} could be calculated from $J_{ph} = qG_{max}L$, where q is the electronic charge and L is the thickness of active layer (124 nm). The values of G_{max} for the control device and device with dual NPs are 8.53×10^{27} m^{-3} s^{-1} ($J_{sat} = 169$ A m^{-2}) and 9.54×10^{27} m^{-3} s^{-1} ($J_{sat} = 190$ A m^{-2}), respectively. An impressive enhancement of G_{max} occurred after incorporation of dual NPs. Since G_{max} is related to maximum absorption of incident photons,[39,40] the enhanced G_{max} suggests increased light absorption in device with dual NPs. The $P(E,T)$ could be obtained from the ratio of J_{ph}/J_{sat}.[31] $P(E,T)$ values under J_{sc} condition increased from 88% in control device to 93% in device with dual NPs, indicating that the excitation of LSPR also benefits the dissociation of excitons into free charge carriers.

Impedance spectroscopy was used to measure the charge carrier density (n) and the effective charge carrier lifetime (τ_{eff}) of our OPV devices.[41,42] In order to evaluate the photogenerated charge carrier density, impedance spectroscopy was measured at V_{oc} condition. At V_{oc} condition, the built-in electric field was canceled out by the applied bias voltage, preventing the photogenerated charge carriers in the active layer from flowing toward electrodes. Thus the possibility of charge recombination at PTB7:$PC_{70}BM$ interface is increased to maximum.[42] Charge carrier density can be calculated based on $n = 1/eAd\int_{dark}^{V_{oc}} C(V)dV$, where e is elementary charge, A is the device area, d is the thickness of the active layer, and C is the chemical capacitance.[42,43] The chemical capacitance is simulated using Schottky equivalent circuit model.[44,45] Figure 4a depicts impedance spectra of PTB7:$PC_{70}BM$ BHJ solar cell with and without dual NPs under simulated 1-sun illumination at V_{oc} condition. From the integration of chemical capacitance over V_{oc} under various illumination intensities, the calculated charge carrier density in device with dual NPs is 1.30×10^{17} cm^{-3}, while the charge carrier density of the control device is 1.13×10^{17} cm^{-3}, it is clear that the incorporating of dual NPs leads to a noticeable enhancement of charge carrier density within the active layer.

Moreover, the τ_{eff} value at J_{sc} condition is extracted from the product of recombination resistance (R_{rec}) and chemical capacitance.[42,46] Impedance spectra of solar cells with and without dual NPs under simulated 1-sun illumination at J_{sc} condition is shown in Figure 4b. The τ_{eff} values of device with dual NPs and the control device are calculated to be 24.38 us and 20.36 us, respectively. In general, a longer τ_{eff} suggests improved charge collection efficiency or decreased charge recombination, or both.[47] To explain the longer τ_{eff} of device with dual NPs, we first measured hole mobility with the structure ITO/PEDOT:PSS with dual NPs/PTB7/Al using space-charge-limited current (SCLC) model.[48] As shown in Figure 4c, hole mobility increased from 5.82×10^{-4} (dark) to 7.00×10^{-4} cm^2 V^{-1} s^{-1} (1-sun illumination) for dual NPs device. The improved hole mobility will lead to improved hole collection efficiency for our OPV devices. To gain deeper insight into the influence of NPs on charge recombination process, the J_{sc} of the control device and dual plasmonic device were measured at various illumination intensities. As shown in Figure 4d, the J_{sc} values of both devices change linearly with light intensity, yielding the same power law of 0.84. Therefore, it can be assumed that incorporation of NPs has negligible influence on charge recombination since the J_{sc} of both devices

dx.doi.org/10.1021/nl3034398 | Nano Lett. 2013, 13, 59–64

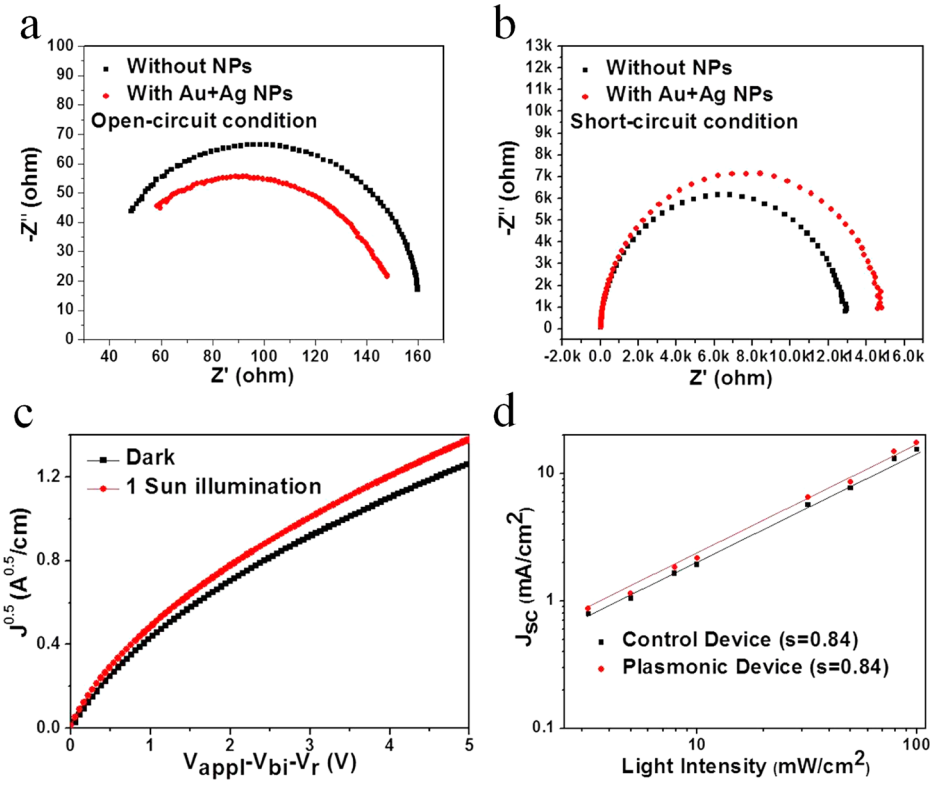

Figure 4. Impedance spectra of PTB7-PCBM BHJ solar cell with/without NPs under 100 mW/cm^2 illumination at (a) open-circuit condition and (b) short-circuit condition. (c) $J^{0.5}$ vs V plots for device with dual NPs under dark and 1 sun illumination. (d) The dependence of J_{sc} on light intensity of PTB7/PC_{70}BM BHJ solar cell with and without dual NPs in PEDOT layer.

show the same dependence on light intensity. Based upon our study on charge transport and recombination, we conjecture that the longer τ_{eff} of device with dual NPs at J_{sc} condition is the result of improved charge transport in the active layer under 1-sun illumination, which is triggered by LSPR of NPs.

The above results indicate that the cooperative plasmonic effect aroused from dual resonance peaks of two different NPs. To better prove this idea, we also prepared devices with Au nanorods (Rod) since Au Rods has dual plamonic resonance peaks itself. On the basis of our results from dual NPs, Au Rods should show superior behavior than Au NPs after blended into PEDOT:PSS buffer layer due to dual LSPR peaks of Au Rods. TEM image of the Au Rods is shown in Figure 5a. The diameter of the rods is around 15 nm and the length is between 40 to 50 nm. The length of Au Rods is almost the same as the size of Au NPs discussed previously in order to minimize the influence of material sizes. The concentration of Au Rods is kept the same as the concentration of the Au NPs under optimized condition. Solar cells with Au Rods were fabricated with the same structure in Figure 1b. Figure 5b depicts the corresponding $J-V$ curve of the device with Au Rods. Compared with Au NPs, the addition of Au Rods into PEDOT:PSS buffer layer further increases J_{sc} to 17.2 mA/cm^2. Average solar cell parameters abstracted over 10 identical devices give mean V_{oc} at 0.71 ± 0.01 V, J_{sc} at 17.1 ± 0.09 mA/cm^2, FF at 69.3 ± 0.64%, and PCE at 8.41 ± 0.07%. EQE spectra of Au Rods device is shown in Figure 5c. The integrated J_{sc} value from the EQE spectra is 16.8 mA/cm^2. Figure 5d shows UV−vis absorption spectrum of PTB7:PC_{70}BM with and without Au Rods. The LSPR peaks of Au Rods in water were located at 515 and 678.5 nm (inset of Figure 5d), respectively. On the basis of EQE and UV−vis absorption spectra, the

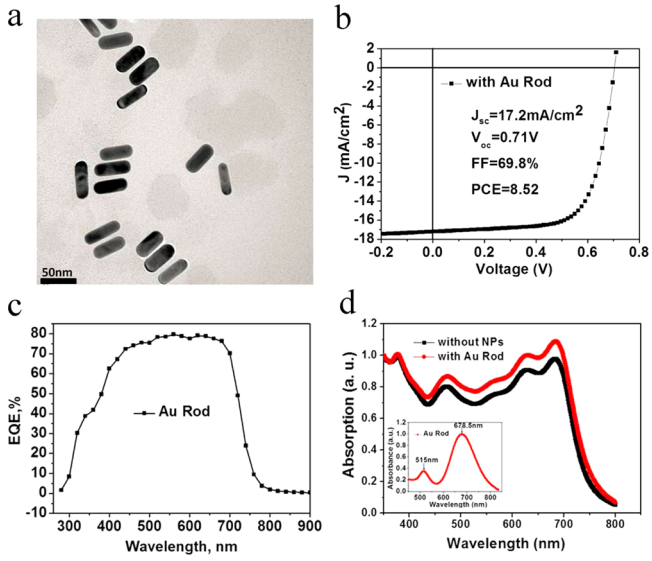

Figure 5. (a) TEM images of Au Rod in water. (b) $J-V$ curve of PTB7/PC_{70}BM with Au Rod. (c) EQE spectra of PTB7/PC_{70}BM with Au Rod. (d) UV−vis absorption spectrum of PTB7/PC_{70}BM with and without Au Rod. Inset: UV−vis absorption spectrum of Au Rod in water.

incorporation of Au Rods into PEDOT:PSS significantly increased the absorption of the active layer in a broad wavelength region from 450 to 720 nm. The further enhanced J_{sc} of devices from Au Rods is in concert with our previous results of dual NPs.

To conclude, we improved the PCEs of BHJ solar cells by incorporating metal NPs into PEDOT:PSS buffer layer. LSPR-

dx.doi.org/10.1021/nl3034398 | *Nano Lett.* 2013, 13, 59−64

induced local field enhancement not only leads to increased light absorption of active layer materials but also benefits charge separation and transport, resulting in increased charge carrier density and lifetime. Moreover, we also show that cooperative plasmonic enhancement could be achieved by simply combining different NPs (i.e., Ag and Au) into PEDOT:PSS buffer layer. The LSPR induced light absorption enhancement region would be much broader after combination, this idea is further proved by solar cell performance of devices with Au Rods. A high PCE of 8.67% was achieved in this way. We believe that the results of our study offer an effective approach to enhance the efficiency of organic BHJ solar cells.

■ ASSOCIATED CONTENT

Ⓢ Supporting Information

This material contains the detailed method for solar cell device preparation and characterization and tables for average solar cell parameters and series resistance. This material is available free of charge via the Internet at http://pubs.acs.org.

■ AUTHOR INFORMATION

Corresponding Author

*E-mail: lupingyu@uchicago.edu.

Notes

The authors declare no competing financial interest.

■ ACKNOWLEDGMENTS

This work is supported by U.S. National Science Foundation Grant (NSF DMR-1004195), Air Force Office of Scientific Research and NSF MRSEC program at the University of Chicago, DOE via the ANSER Center, an Energy Frontier Research Center funded by the U.S. Department of Energy, Office of Science, Office of Basic Energy Sciences, under award number DE-SC0001059. A generous gift from Zhejiang Pharma is also appreciated.

■ REFERENCES

(1) Yu, G.; Gao, J.; Hummelen, J. C.; Wudl, F.; Heeger, A. J. *Science* **1995**, *270*, 1789−1791.
(2) Thompson, B. C.; Frechet, J. M. J. *Angew. Chem., Int. Ed.* **2008**, *47*, 58−77.
(3) Gunes, S.; Neugebauer, H.; Sariciftci, N. S. *Chem. Rev.* **2007**, *107*, 1324−1338.
(4) Hoth, C. N.; Schilinsky, P.; Choulis, S. A.; Brabec, C. J. *Nano Lett.* **2008**, *8*, 2806−2813.
(5) Liang, Y. Y.; Xu, Z.; Xia, J. B.; Tsai, S. T.; Wu, Y.; Li, G.; Ray, C.; Yu, L. P. *Adv. Mater.* **2010**, *22*, E135−E138.
(6) Piliego, C.; Holcombe, T. W.; Douglas, J. D.; Woo, C. H.; Beaujuge, P. M.; Frechet, J. M. J. *J. Am. Chem. Soc.* **2010**, *132*, 7595−7597.
(7) Chu, T. Y.; Lu, J. P.; Beaupre, S.; Zhang, Y. G.; Pouliot, J. R.; Wakim, S.; Zhou, J. Y.; Leclerc, M.; Li, Z.; Ding, J. F.; Tao, Y. *J. Am. Chem. Soc.* **2011**, *133*, 4250−4253.
(8) Saadeh, H. A.; Lu, L.; He, F.; Bullock, J. E.; Wang, W.; Carsten, B.; Yu, L. *ACS Macro Lett.* **2012**, *1*, 361−365.
(9) Price, S. C.; Stuart, A. C.; Yang, L. Q.; Zhou, H. X.; You, W. *J. Am. Chem. Soc.* **2011**, *133*, 4625−4631.
(10) Amb, C. M.; Chen, S.; Graham, K. R.; Subbiah, J.; Small, C. E.; So, F.; Reynolds, J. R. *J. Am. Chem. Soc.* **2011**, *133*, 10062−10065.
(11) Yang, X. N.; Loos, J.; Veenstra, S. C.; Verhees, W. J. H.; Wienk, M. M.; Kroon, J. M.; Michels, M. A. J.; Janssen, R. A. J. *Nano Lett.* **2005**, *5*, 579−583.
(12) Campbell, A. R.; Hodgkiss, J. M.; Westenhoff, S.; Howard, I. A.; Marsh, R. A.; McNeill, C. R.; Friend, R. H.; Greenham, N. C. *Nano Lett.* **2008**, *8*, 3942−3947.
(13) Lou, S. J.; Szarko, J. M.; Xu, T.; Yu, L. P.; Marks, T. J.; Chen, L. X. *J. Am. Chem. Soc.* **2011**, *133*, 20661−20663.
(14) Lee, J. K.; Ma, W. L.; Brabec, C. J.; Yuen, J.; Moon, J. S.; Kim, J. Y.; Lee, K.; Bazan, G. C.; Heeger, A. J. *J. Am. Chem. Soc.* **2008**, *130*, 3619−3623.
(15) Peet, J.; Kim, J. Y.; Coates, N. E.; Ma, W. L.; Moses, D.; Heeger, A. J.; Bazan, G. C. *Nat. Mater.* **2007**, *6*, 497−500.
(16) Wang, D. H.; Moon, J. S.; Seifter, J.; Jo, J.; Park, J. H.; Park, O. O.; Heeger, A. J. *Nano Lett.* **2011**, *11*, 3163−3168.
(17) Lobez, J. M.; Andrew, T. L.; Bulovic, V.; Swager, T. M. *ACS Nano* **2012**, *6*, 3044−3056.
(18) Chen, D. A.; Nakahara, A.; Wei, D. G.; Nordlund, D.; Russell, T. P. *Nano Lett.* **2011**, *11*, 561−567.
(19) Moon, J. S.; Takacs, C. J.; Cho, S.; Coffin, R. C.; Kim, H.; Bazan, G. C.; Heeger, A. J. *Nano Lett.* **2010**, *10*, 4005−4008.
(20) He, X. M.; Gao, F.; Tu, G. L.; Hasko, D.; Huttner, S.; Steiner, U.; Greenham, N. C.; Friend, R. H.; Huck, W. T. S. *Nano Lett.* **2010**, *10*, 1302−1307.
(21) Yang, L. Q.; Zhou, H. X.; Price, S. C.; You, W. *J. Am. Chem. Soc.* **2012**, *134*, 5432−5435.
(22) Kim, J. Y.; Lee, K.; Coates, N. E.; Moses, D.; Nguyen, T. Q.; Dante, M.; Heeger, A. J. *Science* **2007**, *317*, 222−225.
(23) Khlyabich, P. P.; Burkhart, B.; Thompson, B. C. *J. Am. Chem. Soc.* **2011**, *133*, 14534−14537.
(24) Small, C. E.; Chen, S.; Subbiah, J.; Amb, C. M.; Tsang, S. W.; Lai, T. H.; Reynolds, J. R.; So, F. *Nat. Photonics* **2012**, *6*, 115−120.
(25) He, Z. C.; Zhong, C. M.; Huang, X.; Wong, W. Y.; Wu, H. B.; Chen, L. W.; Su, S. J.; Cao, Y. *Adv. Mater.* **2011**, *23*, 4636−4643.
(26) Dou, L. T.; You, J. B.; Yang, J.; Chen, C. C.; He, Y. J.; Murase, S.; Moriarty, T.; Emery, K.; Li, G.; Yang, Y. *Nat. Photonics* **2012**, *6*, 180−185.
(27) Li, G.; Zhu, R.; Yang, Y. *Nat. Photonics* **2012**, *6*, 153−161.
(28) Blom, P. W. M.; Mihailetchi, V. D.; Koster, L. J. A.; Markov, D. E. *Adv. Mater.* **2007**, *19*, 1551−1566.
(29) Atwater, H. A.; Polman, A. *Nat. Mater.* **2010**, *9*, 205−213.
(30) Wang, D. H.; Kim, D. Y.; Choi, K. W.; Seo, J. H.; Im, S. H.; Park, J. H.; Park, O. O.; Heeger, A. J. *Angew. Chem., Int. Ed.* **2011**, *50*, 5519−5523.
(31) Wu, J. L.; Chen, F. C.; Hsiao, Y. S.; Chien, F. C.; Chen, P. L.; Kuo, C. H.; Huang, M. H.; Hsu, C. S. *ACS Nano* **2011**, *5*, 959−967.
(32) Yang, J.; You, J. B.; Chen, C. C.; Hsu, W. C.; Tan, H. R.; Zhang, X. W.; Hong, Z. R.; Yang, Y. *ACS Nano* **2011**, *5*, 6210−6217.
(33) Wang, C. C. D.; Choy, W. C. H.; Duan, C. H.; Fung, D. D. S.; Sha, W. E. I.; Xie, F. X.; Huang, F.; Cao, Y. *J. Mater. Chem.* **2012**, *22*, 1206−1211.
(34) Heo, M.; Cho, H.; Jung, J. W.; Jeong, J. R.; Park, S.; Kim, J. Y. *Adv. Mater.* **2011**, *23*, 5689−5693.
(35) Wang, D. H.; Park, K. H.; Seo, J. H.; Seifter, J.; Jeon, J. H.; Kim, J. K.; Park, J. H.; Park, O. O.; Heeger, A. J. *Adv. Energy Mater.* **2011**, *1*, 766−770.
(36) Stavytska-Barba, M.; Salvador, M.; Kulkarni, A.; Ginger, D. S.; Kelley, A. M. *J. Phys. Chem. C* **2011**, *115*, 20788−20794.
(37) Li, X. H.; Choy, W. C. H.; Huo, L. J.; Xie, F. X.; Sha, W. E. I.; Ding, B. F.; Guo, X.; Li, Y. F.; Hou, J. H.; You, J. B.; Yang, Y. *Adv. Mater.* **2012**, *24*, 3046−3052.
(38) Mihailetchi, V. D.; Wildeman, J.; Blom, P. W. M. *Phys. Rev. Lett.* **2005**, *94*, 126602.
(39) Mihailetchi, V. D.; Koster, L. J. A.; Hummelen, J. C.; Blom, P. W. M. *Phys. Rev. Lett.* **2004**, *93*, 216601.
(40) Shuttle, C. G.; Hamilton, R.; O'Regan, B. C.; Nelson, J.; Durrant, J. R. *Proc. Natl. Acad. Sci. U.S.A.* **2010**, *107*, 16448−16452.
(41) Kuwabara, T.; Kawahara, Y.; Yamaguchi, T.; Takahashi, K. *ACS Appl. Mater. Interfaces* **2009**, *1*, 2107−2110.
(42) Leever, B. J.; Bailey, C. A.; Marks, T. J.; Hersam, M. C.; Durstock, M. F. *Adv. Energy Mater.* **2012**, *2*, 120−128.
(43) Shuttle, C. G.; O'Regan, B.; Ballantyne, A. M.; Nelson, J.; Bradley, D. D. C.; de Mello, J.; Durrant, J. R. *Appl. Phys. Lett.* **2008**, *92*, 093311.

(44) Garcia-Belmonte, G.; Munar, A.; Barea, E. M.; Bisquert, J.; Ugarte, I.; Pacios, R. *Org. Electron.* **2008**, *9*, 847−851.
(45) Garcia-Belmonte, G.; Boix, P. P.; Bisquert, J.; Sessolo, M.; Bolink, H. J. *Sol. Energy Mater. Sol. Cells* **2010**, *94*, 366−375.
(46) Street, R. A.; Schoendorf, M. *Phys. Rev. B* **2010**, *81*, 205307.
(47) Zhang, Y.; Dang, X. D.; Kim, C.; Nguyen, T. Q. *Adv. Energy Mater.* **2011**, *1*, 610−617.
(48) Goh, C.; Kline, R. J.; McGehee, M. D.; Kadnikova, E. N.; Frechet, J. M. J. *Appl. Phys. Lett.* **2005**, *86*, 122110.

dx.doi.org/10.1021/nl3034398 | *Nano Lett.* 2013, 13, 59−64